



## OPEN ACCESS

EDITED BY  
Octavian-Dumitru Pavel,  
University of Bucharest, Romania

REVIEWED BY  
Luis F. Bobadilla,  
University of Seville, Spain  
Matthijs Ruitenbeek,  
Dow Benelux, Netherlands

\*CORRESPONDENCE  
Christina Charalambous,  
christina.charalambous@  
manchester.ac.uk  
Shanshan Xu,  
shanshan.xu@manchester.ac.uk  
Arthur Garforth,  
arthur.garforth@manchester.ac.uk  
Christopher Hardacre,  
c.hardacre@manchester.ac.uk

SPECIALTY SECTION  
This article was submitted  
to Catalytic Engineering,  
a section of the journal  
Frontiers in Chemical Engineering

RECEIVED 24 August 2022  
ACCEPTED 31 October 2022  
PUBLISHED 15 November 2022

CITATION  
Charalambous C, Xu S, Ding S,  
Chansai S, Asuquo E, Torres Lopez A,  
Parlett CMA, Gilmour JD, Garforth A and  
Hardacre C (2022), Non-thermal plasma  
activated CO<sub>2</sub> hydrogenation over K-  
and La- promoted layered-double  
hydroxide supported Ni catalysts.  
*Front. Chem. Eng.* 4:1027167.  
doi: 10.3389/fceng.2022.1027167

COPYRIGHT  
© 2022 Charalambous, Xu, Ding,  
Chansai, Asuquo, Torres Lopez,  
Parlett, Gilmour, Garforth and  
Hardacre. This is an open-access  
article distributed under the terms  
of the [Creative Commons Attribution  
License \(CC BY\)](#). The use,  
distribution or reproduction in  
other forums is permitted, provided  
the original author(s) and the  
copyright owner(s) are credited  
and that the original publication  
in this journal is cited, in  
accordance with accepted  
academic practice. No use,  
distribution or reproduction is  
permitted which does not comply  
with these terms.

# Non-thermal plasma activated CO<sub>2</sub> hydrogenation over K- and La- promoted layered-double hydroxide supported Ni catalysts

Christina Charalambous<sup>1\*</sup>, Shanshan Xu<sup>1\*</sup>, Shengzhe Ding<sup>1</sup>,  
Sarayute Chansai<sup>1</sup>, Edidiong Asuquo<sup>2</sup>, Antonio Torres Lopez<sup>1,3</sup>,  
Christopher M. A. Parlett<sup>1,3,4</sup>, Jamie D. Gilmour<sup>5</sup>,  
Arthur Garforth<sup>1\*</sup> and Christopher Hardacre<sup>1\*</sup>

<sup>1</sup>Department of Chemical Engineering, School of Engineering, The University of Manchester, Manchester, United Kingdom, <sup>2</sup>Department of Chemical Engineering and Analytical Science, Faculty of Science and Engineering, The University of Manchester, Manchester, United Kingdom, <sup>3</sup>Catalysis Hub, Research Complex at Harwell, Rutherford Appleton Laboratory, Harwell, United Kingdom, <sup>4</sup>Diamond Light Source, Harwell Campus, Didcot, United Kingdom, <sup>5</sup>Department of Earth and Environmental Sciences, School of Natural Sciences, The University of Manchester, Manchester, United Kingdom

The catalytic conversion of CO<sub>2</sub> to CH<sub>4</sub> and CO over nickel particles supported on layered-double hydroxide (MgAl) with different metal promoters was investigated under non-thermal plasma (NTP) conditions. It has been shown that lanthanum-promoted Ni catalysts significantly enhanced the CO<sub>2</sub> conversion in comparison to the 10Ni/MgAl catalyst (33.4% vs. 89.3%). In comparison, for the potassium-promoted catalysts, CO<sub>2</sub> conversion is similar to that of 10Ni/MgAl but the CO selectivity increased significantly (35.7% vs. 62.0%). The introduction of La and K to Ni catalysts increased the Ni dispersion and improved the reducibility of Ni species, thus affecting CO<sub>2</sub> conversion and product selectivity. *In situ* DRIFTS showed similar reaction pathways for La- and K- promoted catalysts with Ni catalysts. However, the La and K promoters significantly improved the formation of formate species on the Ni surface, facilitating CO<sub>2</sub> conversion to useful products.

## KEYWORDS

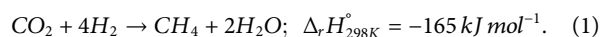
non-thermal plasma (NTP), CO<sub>2</sub> hydrogenation, layered double hydroxides, fine chemicals, catalyst support, promoter

## 1 Introduction

The catalytic conversion of CO<sub>2</sub> into useful chemicals (CO, CH<sub>4</sub>, CH<sub>3</sub>OH) has attracted attention due to the ongoing environmental crisis and the requirement for new technologies for space exploration. CO<sub>2</sub> methanation, also known as the Sabatier reaction, is a potential pathway for the generation of methane and its subsequent use as fuel (the “power-to-gas” concept) for renewable energy (George et al., 2021). Additionally, in 2011, the Sabatier-Electrolysis process was used at the International Space Station to recycle oxygen from waste CO<sub>2</sub>, via water production (Samplatsky et al.; Petersen, 2019). The

process helped to reduce the amount of oxygen required to be transported in the form of liquid water and, therefore, cut down the launch expenses considerably. Recently, CO<sub>2</sub> hydrogenation is considered a means of producing cryogenic propellant (liquid CH<sub>4</sub>/liquid oxygen) and can contribute to long-term space exploration missions (Vogt et al., 2019). Therefore, the development of new catalysts as well as investigation of efficient processes for CO<sub>2</sub> hydrogenation is still needed.

Traditionally, CO<sub>2</sub> hydrogenation involves high temperatures and/or pressures to overcome the kinetically limited activation of CO<sub>2</sub> molecules under thermal conditions. Alternative ways for CO<sub>2</sub> conversion include photocatalysis, electrocatalysis, and plasma-catalysis (Tu et al., 2014; Du et al., 2020; Chen et al., 2021). Hybrid non-thermal plasma (NTP) and catalysis systems (NTP-catalysis) enable the activation of stable CO<sub>2</sub> molecules and promote catalytic CO<sub>2</sub> conversion at relatively mild bulk temperatures and atmospheric pressure. This is in contrast to conventional thermal catalysis and promises energy-efficient conversion of CO<sub>2</sub> into CH<sub>4</sub> and CO (Whitehead, 2016; Bogaerts and Centi, 2020; Chen et al., 2020).



The catalyst design for CO<sub>2</sub> hydrogenation has been intensively investigated, (Benrabbah et al., 2017; Chen et al., 2019; Da Costa et al., 2021) and Ni-based catalysts are widely used due to their low cost (Li et al., 2018). However, the nature of the supporting material (e.g., surface area, surface modification, and metal-support interactions) has been demonstrated to play a key role in terms of promoting CO<sub>2</sub> conversion. Metal species, such as K, Na, La, and Ce, have been employed as promoters to increase CO<sub>2</sub> adsorption under thermal conditions, which is beneficial for CO<sub>2</sub> conversion (Cimino et al., 2020; Kumar et al., 2021). Additionally, alkali metal (Na, K, Li)-modified hydrotalcite catalysts have been applied to biogas dry reforming where the catalyst deactivation rate was found to be dependent on the metal used with deactivation found to be higher down the group (Rosset et al., 2021). These findings were attributed to the higher reduction temperature and resistance to metal sintering for the Li-promoted catalyst (Rosset et al., 2021). Zeng et al. (2018) showed that the K-promoted Ni/Al<sub>2</sub>O<sub>3</sub> catalyst showed increased conversion and improved energy efficiency compared to the unpromoted catalyst due to enhanced acidity which contributes to CH<sub>4</sub> activation. In plasma-catalytic CO<sub>2</sub> hydrogenation, the effect of promoters on the structure and performance of Ni catalysts has not been investigated to the same extent. Therefore, a systematic investigation of the promoter modification-structure-performance relationships in the supported Ni catalysts is needed for the rational development of highly-efficient catalysts for plasma catalysis. Specifically, K and La have been reported to increase CO<sub>2</sub> chemisorption and surface basicity, as well as improve metal dispersion (Choi et al., 1996; Kumar et al., 2021). Layered double hydroxides (LDHs), also

known as anionic clays, consist of 2D brucite-like layers of positively charged ions with host molecules and anions in the interlayer space (He et al., 2013). Their coordinated hydroxyl (–OH) group can increase CO<sub>2</sub> chemisorption, high ion-exchange capacity, and unsaturated active sites for improved metal dispersion (He et al., 2013; Xu et al., 2020), making them promising as catalysts, catalyst precursors and catalyst supports.

In this work, a series of La- and K- promoted Ni catalysts supported on MgAl LDHs have been examined for CO<sub>2</sub> hydrogenation under NTP conditions in a dielectric barrier (DBD) reactor. Specifically, we investigated 1) the performance of NTP-assisted CO<sub>2</sub> hydrogenation of Ni/MgAl in comparison to the control experiments (i.e., catalyst-free system and the inert material); 2) the effect of rare Earth metals (La) and alkali metals (K) on CO<sub>2</sub> conversion and CO/CH<sub>4</sub> selectivity and 3) the mechanism of NTP-assisted CO<sub>2</sub> hydrogenation by using *in situ* diffuse reflectance infrared Fourier transform spectroscopy-mass spectrometry (DRIFTS-MS).

## 2 Materials and methods

### 2.1 Chemicals

MgAl hydrotalcite, nickel nitrate hexahydrate (Ni(NO<sub>3</sub>)<sub>2</sub>·6H<sub>2</sub>O (99.98%)) and lanthanum nitrate hexahydrate (La(NO<sub>3</sub>)<sub>3</sub>·6H<sub>2</sub>O (99.999%)) were purchased from Sigma Aldrich. Potassium nitrate (KNO<sub>3</sub>) was purchased from Alfa Aesar. All chemicals were used as received.

### 2.2 Catalyst preparation

The wet impregnation method was used to prepare the Ni catalysts. The MgAl hydrotalcite support was added to a solution of Ni(NO<sub>3</sub>)<sub>2</sub>·6H<sub>2</sub>O under vigorous stirring. The Ni metal loading was kept at 10 wt%. The suspension was stirred at 60°C until dryness. After impregnation, the catalysts were further dried at 100°C overnight, followed by calcination at 550°C with a ramp rate of 2°C min<sup>-1</sup>. In the case where a promoter was used (La, K), the corresponding metal salt (La(NO<sub>3</sub>)<sub>3</sub>·6H<sub>2</sub>O and KNO<sub>3</sub>) was impregnated together with Ni(NO<sub>3</sub>)<sub>2</sub>·6H<sub>2</sub>O in a one-pot method to achieve 1, 3 and 5 wt% of La and 0.5, 1 and 3 wt% of K. The catalysts were pressed and sieved (250–425 μm) and reduced at 500°C for 2 h using pure H<sub>2</sub>. The samples are termed as 10Ni-xM/MgAl where x represents the wt% loading of the promoting metal, and M is either La or K.

### 2.3 Characterisation of the catalysts

The structure of the catalysts was determined by X-Ray Diffraction (XRD) on a BrukerD8 Discover AutoChanger

diffractometer with  $\text{CuK}_{\alpha 1}$  radiation ( $\lambda = 1.5406 \text{ \AA}$ ). Diffractograms were recorded from  $5$  to  $90^\circ$  at a  $0.02^\circ$  step size.

Hydrogen temperature-programmed reduction ( $\text{H}_2$ -TPR) and  $\text{CO}_2$  temperature-programmed desorption ( $\text{CO}_2$ -TPD) were carried out using a Quantachrome ChemBET Pulsar TPR/TPD instrument. For the  $\text{H}_2$ -TPR,  $35 \text{ mg}$  of catalyst were pre-treated at  $200^\circ\text{C}$  for  $1 \text{ h}$  under argon to remove adsorbed  $\text{H}_2\text{O}$  and  $\text{CO}_2$  on the catalyst surface. The sample was cooled to room temperature and the  $\text{H}_2$ -TPR was carried out under a gas flow of  $5\% \text{ H}_2$  in Ar from  $30$  to  $900^\circ\text{C}$  ( $10^\circ\text{C min}^{-1}$ ). The  $\text{H}_2$  consumption was monitored using a thermal conductivity detector (TCD). Prior to  $\text{CO}_2$ -TPD, the samples were pre-treated with  $5\% \text{ H}_2/\text{Ar}$  at  $250^\circ\text{C}$  for  $50 \text{ min}$  and cooled to room temperature.  $\text{CO}_2$  was introduced on the catalyst surface for  $90 \text{ min}$  to ensure saturated  $\text{CO}_2$  adsorption and then the samples were purged using Ar for  $40 \text{ min}$ . TPD analysis was performed from  $30$  to  $800^\circ\text{C}$  ( $10^\circ\text{C min}^{-1}$ ) and the  $\text{CO}_2$  desorption was monitored using a TCD.

Transmission electron microscopy (TEM) was conducted using a FEI Talos F200A-AEM TEM operating at  $200 \text{ kV}$ , equipped with a Schottky field-emission gun (X-FEG) and an FEI Super-X4-detector EDX system.

Thermogravimetric analysis (TGA) on the spent catalyst was carried out using a Discovery TGA 550 (TA Instruments). Under flowing  $\text{N}_2$  ( $40 \text{ ml min}^{-1}$ ), samples were heated to  $550^\circ\text{C}$  at  $10^\circ\text{C min}^{-1}$  and then held for  $180 \text{ min}$  to equilibrate. Thereafter, the gas flow was switched to air ( $40 \text{ ml min}^{-1}$ ) and held at  $550^\circ\text{C}$  for  $180 \text{ min}$  to oxidise the remaining carbonaceous material.

Analysis of the actual metal content in each catalyst was carried out using a Quant PQ900 Inductively Coupled Plasma Optical Emission Spectrometer (ICP-OES). All catalysts ( $20 \text{ mg}$ ) were pre-treated with microwave digestion in  $12 \text{ ml}$  aqua regia at  $220^\circ\text{C}$  using an ETHOS UP microwave digester.

X-Ray photoelectron spectrometer (XPS; Kratos AXIS Ultra DLD), equipped with a monochromated Al  $\text{K}_{\alpha}$  radiation X-Ray source ( $1,486.6 \text{ eV}$ ), a charge neutralizer, and a hemispherical electron energy analyser were used to perform valence state analysis on Ni samples. In all cases, XPS spectra were taken for Ni 2p, O 1s, and C 1s. The XPS spectra were processed using Casa XPS (Version 2.3.19PR1.0). All samples were calibrated with respect to the adventitious carbon 1s peak at  $284.6 \text{ eV}$ .

## 2.4 NTP-assisted $\text{CO}_2$ hydrogenation

$\text{CO}_2$  hydrogenation was carried out in a dielectric barrier discharge (DBD) reactor. The experimental setup is shown in Supplementary Figure S1. Typically,  $100 \text{ mg}$  of catalyst ( $250\text{--}425 \mu\text{m}$ ) was packed into a quartz tube reactor (I.D.  $4 \text{ mm}$ , O.D.  $6 \text{ mm}$ ) and held in the discharge space by two quartz wool plugs. The ground electrode was placed in the centre of the reactor, and the high voltage electrode was

wrapped around the outside of the quartz reactor. The experiments were carried out at atmospheric pressure. Prior to the reaction, the catalyst was pretreated *in situ* under NTP with  $\text{H}_2$  ( $6 \text{ kV}$ ,  $20.8 \text{ kHz}$ ) for  $20 \text{ min}$ . Subsequently, the reaction gas feed ( $\text{H}_2/\text{CO}_2/\text{Ar} = 4:1:5$ ) was introduced inside the reactor at  $50 \text{ ml min}^{-1}$ . The DBD reactor was connected to an alternating current (AC) high voltage power supply. All experiments were carried out at  $20.8 \text{ kHz}$  while the voltage varied from  $5.5$  to  $7 \text{ kV}$ . The peak voltage was monitored by a digital oscilloscope and the outlet gases were detected by an on-line gas chromatograph (GC) equipped with a Hayesep DB column, TCD and flame-ionisation detector (FID). The average temperature of the DBD reactor varied from  $100$  to  $120^\circ\text{C}$  (measured by an IR gun). Liquid products were condensed by using a glass water trap cooled by an ice bath. The  $\text{CO}_2$  conversion,  $\text{CH}_4$  selectivity and CO selectivity were calculated using Eqs 2, 3 and 4. The energy efficiency (EE) ( $\text{mmol kJ}^{-1}$ ) and specific energy input (SEI) ( $\text{kJ L}^{-1}$ ) were calculated using Eqs 5, 6.

$$X_{\text{CO}_2} = \frac{F_{\text{CO}_2}^{\text{in}} - F_{\text{CO}_2}^{\text{out}}}{F_{\text{CO}_2}^{\text{in}}} \times 100, \quad (2)$$

where  $F_{\text{CO}_2}^{\text{in}}$  and  $F_{\text{CO}_2}^{\text{out}}$  are the molar flow rates ( $\text{mol s}^{-1}$ ) of  $\text{CO}_2$  in the inlet and outlet of the DBD reactor, respectively.

$$S_{\text{CH}_4} = \frac{F_{\text{CH}_4}^{\text{out}}}{F_{\text{CO}_2}^{\text{in}} - F_{\text{CO}_2}^{\text{out}}} \times 100, \quad (3)$$

$$S_{\text{CO}} = \frac{F_{\text{CO}}^{\text{out}}}{F_{\text{CO}_2}^{\text{in}} - F_{\text{CO}_2}^{\text{out}}} \times 100, \quad (4)$$

where  $F_{\text{CH}_4}^{\text{out}}$  and  $F_{\text{CO}}^{\text{out}}$  are the molar flow rates ( $\text{mol s}^{-1}$ ) of  $\text{CH}_4$  and CO at the outlet of the DBD reactor.

$$EE = \frac{\text{moles of CH}_4 \text{ produced} + \text{moles of CO produced}}{\text{power}_{\text{DBD}}}, \quad (5)$$

$$SEI = \frac{\text{power}_{\text{DBD}}}{F_{\text{total}}}, \quad (6)$$

where moles of  $\text{CH}_4$  and CO produced are in units of  $\text{mmol s}^{-1}$ ,  $\text{power}_{\text{DBD}}$  is the discharge power (kW) and  $F_{\text{total}}$  is the total flow rate ( $50 \text{ ml min}^{-1}$ ).

## 2.5 *In situ* DRIFTS characterisation

The surface species adsorbed on the catalyst surface during the NTP-assisted  $\text{CO}_2$  hydrogenation were studied using *in situ* DRIFTS-MS analysis. The detailed structure and setup of the *in situ* DRIFTS cell for NTP catalysis were described elsewhere (Stere et al., 2020). *In situ* DRIFTS measurements were performed using a Bruker Vertex 70 FTIR spectrometer, equipped with a liquid  $\text{N}_2$ -cooled mercury-cadmium-telluride (MCT) detector. Typically,  $50 \text{ mg}$  of catalyst were loaded into the infrared sample cell and pre-treated under  $20\% \text{ H}_2/\text{Ar}$  at  $5 \text{ kV}$  and  $27.2 \text{ kHz}$  for  $10 \text{ min}$ . Then

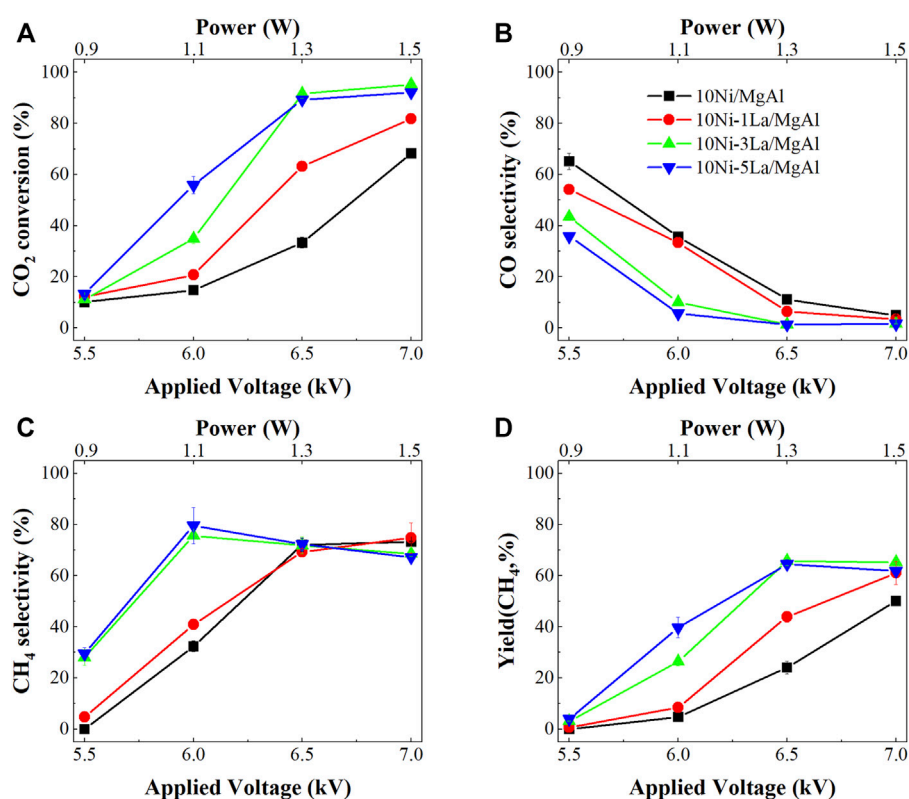


FIGURE 1

Performance of NTP-assisted CO<sub>2</sub> hydrogenation as a function of voltage over the 10Ni/MgAl system with different loadings of La; (A) CO<sub>2</sub> conversion, (B) CO selectivity, (C) CH<sub>4</sub> selectivity and (D) CH<sub>4</sub> yield.

the gas feed ( $H_2/CO_2 = 4$  diluted in 90% Ar) at  $60 \text{ ml min}^{-1}$  was introduced into the cell. The use of Ar balance in DRIFTS was to avoid the signal saturation of IR spectra and MS signal. For the experiment, an applied voltage of 5 kV and frequency of 27.2 kHz was used to prevent arcing. DRIFTS spectra were recorded every 30 s and analysed by the OPUS software. During the experiment, mass spectrometry (Hiden Analytical HPR20) was employed to analyse gases ( $CO_2$ , CO,  $CH_4$ ) that exit the DRIFTS cell (shown in the SI).

### 3 Results and discussion

#### 3.1 NTP-assisted CO<sub>2</sub> hydrogenation

The performance of various Ni/MgAl catalysts in NTP-assisted CO<sub>2</sub> hydrogenation was studied in comparison to the control experiments (i.e., empty reactor for gas phase reaction and with the MgAl packing under NTP conditions). The catalyst-free system and the MgAl packing system showed a low CO<sub>2</sub> conversion of <15% and 100% selectivity to CO (Supplementary Figure S2) regardless of the applied power, which can be

attributed to gas phase dissociation of CO<sub>2</sub> to CO under NTP conditions (George et al., 2021). In contrast, when the NTP was packed with the 10Ni/MgAl catalyst, the plasma-catalyst system showed significantly higher activity, demonstrating the synergy between the catalyst and NTP. Specifically, CO<sub>2</sub> conversion and CH<sub>4</sub> selectivity increased with applied voltage/power, which is due to higher specific energy input facilitating CO<sub>2</sub> activation and methane formation. The highest CO<sub>2</sub> conversion and CH<sub>4</sub> selectivity of 68.3% and 73.3% were achieved, respectively, by the 10Ni/MgAl catalyst at the applied power of 1.5 W (corresponding to a SEI of  $1.8 \text{ kJ L}^{-1}$ ).

Compared to the 10Ni/MgAl catalyst, the addition of lanthanum as a promoter significantly enhanced CO<sub>2</sub> conversion under NTP conditions over all the La-promoted Ni catalysts (Figure 1). Specifically, with the La loading increasing from 1 wt% to 5 wt%, CO<sub>2</sub> conversion and CH<sub>4</sub> selectivity showed a steady increasing trend at the applied power of <1.3W (SEI of  $1.6 \text{ kJ L}^{-1}$ ). For example, at 6 kV (i.e., 1.1 W and SEI of  $1.3 \text{ kJ L}^{-1}$ ), the CO<sub>2</sub> conversion and CH<sub>4</sub> selectivity increased from 20.7% to 55.9% and from 40.8% to 79.6%, respectively, over 10Ni-5La/MgAl catalyst. With the applied voltage further increasing to 7 kV

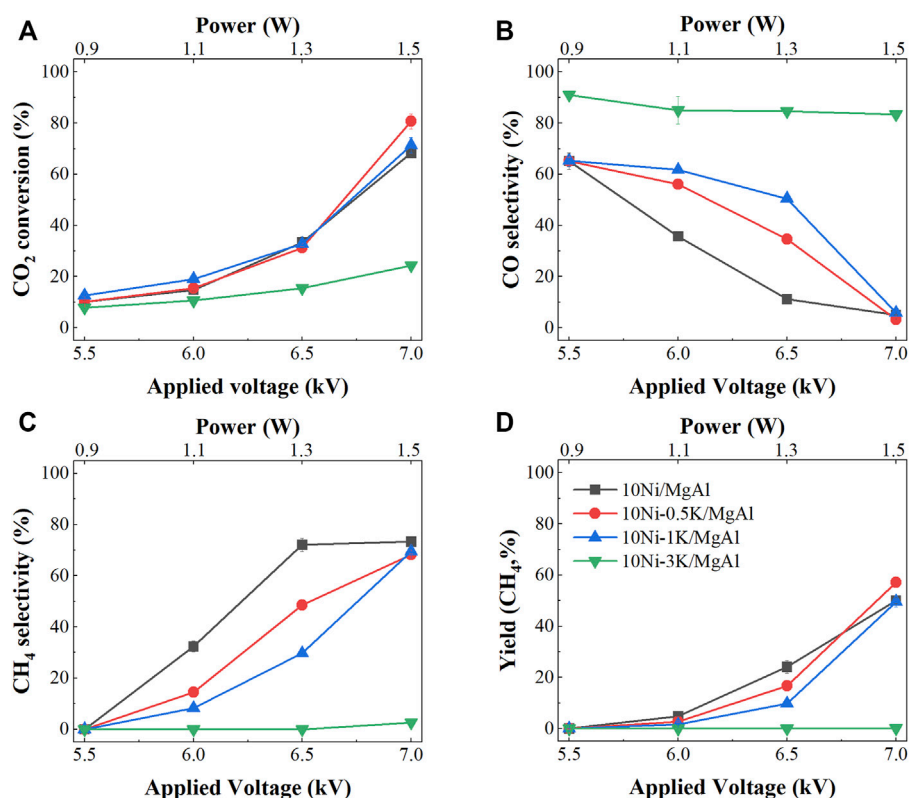


FIGURE 2

Performance of NTP-assisted CO<sub>2</sub> hydrogenation as a function of voltage over the 10Ni/MgAl system with different loadings of K; (A) CO<sub>2</sub> conversion, (B) CO selectivity, (C) CH<sub>4</sub> selectivity and (D) CH<sub>4</sub> yield.

(i.e., 1.5 W and SEI of 1.8 kJ L<sup>-1</sup>), CO<sub>2</sub> conversion over the 10Ni-3La/MgAl and 10Ni-5La/MgAl catalysts increased to 95.2% and 92.1%, while the CH<sub>4</sub> selectivity dropped to 68.5 and 67.2%, respectively. This can be attributed to the formation of C<sub>2</sub> products due to methane coupling under high plasma power, as shown in the supplementary information (Supplementary Figure S3). The 10Ni-5La/MgAl catalyst showed the best activity for NTP-activated CO<sub>2</sub> hydrogenation with maximum CO<sub>2</sub> conversion and CH<sub>4</sub> selectivity of 89.3% and 72.3% at 1.3 W (SEI of 1.6 kJ L<sup>-1</sup>), respectively.

In comparison, K-promoted catalysts showed no improvement in CO<sub>2</sub> conversions but had significantly increased CO selectivity (Figure 2). For 10Ni-0.5K/MgAl and 10Ni-1K/MgAl catalysts, CO<sub>2</sub> conversion remained comparable with that of 10Ni/MgAl catalyst which increased with applied power reaching a maximum CO<sub>2</sub> conversion of ~70% at 1.5 W. However, the CO selectivity was enhanced by 20.3% and 26% at 1.1 W (SEI of 1.3 kJ L<sup>-1</sup>) and by 23.4% and 39.2% at 1.3 W (SEI of 1.6 kJ L<sup>-1</sup>), respectively, compared to the 10Ni/MgAl catalyst. For example, 10Ni-1K/MgAl catalyst showed a CO selectivity of 62% at 1.1 W (SEI of 1.3 kJ L<sup>-1</sup>), while 10Ni/MgAl catalyst only had a selectivity of 35.7%. At the high applied power of 1.5 W (SEI of

1.8 kJ L<sup>-1</sup>), the CO selectivity dropped to ~6% and the CH<sub>4</sub> selectivity increased to ~70% for both catalysts, which is due to the preferred formation of methane from CO with hydrogen under high power of plasma. For the 3 wt% K-promoted catalyst, the CO<sub>2</sub> conversions were significantly lower and showed similar activities with the catalyst-free and support-packing systems and only CO as the product was observed.

### 3.2 Catalyst characterisation

The properties of the catalyst are important in NTP-catalysis as they affect the metal dispersion, adsorption/desorption properties and plasma discharge (Xu et al., 2021). To understand the effect of La and K promoters on the activity of Ni catalysts, extensive characterisation was carried out to investigate the properties of each catalyst, which can be correlated with the apparent activity in CO<sub>2</sub> hydrogenation under NTP conditions.

Figure 3, Supplementary Figure S5 showed the XRD patterns of La- and K-modified catalysts in comparison to the 10Ni/MgAl and MgAl support. In Supplementary Figure S5, characteristic peaks at 11.7, 23.4, 34.9 and 39.5°, corresponding to the (003),

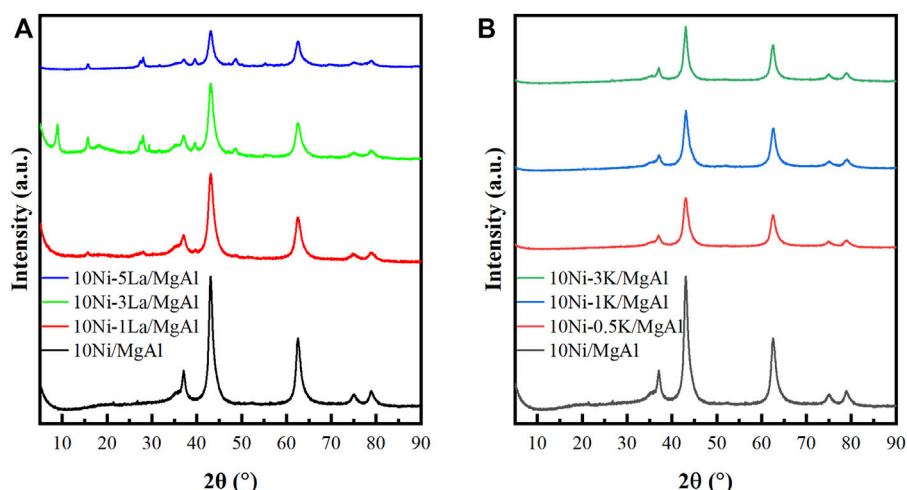


**FIGURE 3**  
XRD patterns of reduced (A) La- and (B) K-modified catalysts.

(006), (012) and (015) reflections of the well-defined hydrotalcite structure (JCPDS Card No. 1-82-8043), were observed for the MgAl support (Xu et al., 2020). The basal spacing ( $d_{003}$ ) of the MgAl support was calculated to be 0.8 nm. Supplementary Table S1 contains the lattice parameters and crystallite sizes of the fresh and spent catalysts.

In Figure 3, the 10Ni/MgAl catalyst showed no peaks for the hydrotalcite structure, indicating that upon calcination, the crystalline structure of layered double hydroxide had collapsed and converted to the layered double oxide (LDO) structure. After reduction, characteristic peaks of NiO at  $2\theta = 37.1, 43.1, 62.4, 75.2$  and  $78.9^\circ$  corresponding to the (111), (200), (220), (311), and (222) crystal planes of the bulk NiO (JCPDS Card No. 01-071-4750) were observed over the Ni/MgAl catalyst, indicating that the Ni species were not fully reduced at  $500^\circ\text{C}$  or the catalysts were re-oxidised by exposure to air during analysis (Wei et al., 2009). Additionally, characteristic peaks at  $2\theta = 36.9, 44.8$  and  $74.1^\circ$  correspond to the formation of magnesium aluminate spinel ( $\text{MgAl}_2\text{O}_4$ ) (JCPDS Card No. 21-1152) and nickel aluminate spinel ( $\text{NiAl}_2\text{O}_4$ ) (JCPDS Card No. 10-0339) but are difficult to differentiate as they overlap with NiO reflections (Sahli et al., 2006; Touahra et al., 2016; Ranjbar et al., 2019; Warmuz and Madej, 2022). Upon addition of La and K, the intensity of the NiO peaks decreased and the peaks become broader, suggesting a smaller nickel crystallite size and higher dispersion of Ni in La-/K- promoted catalysts compared with the 10Ni/MgAl catalyst. According to the Scherrer equation, the NiO crystallite size in 10Ni/MgAl is estimated to be 8.1 nm, while it decreases to 7.5 nm and 6.5 nm for 10Ni-5La/MgAl and 10Ni-1K/MgAl, respectively. In addition, the peaks at  $28.1, 39.7$  and  $48.7^\circ$  in the La-modified Ni catalysts correspond to the  $\text{La}_2\text{O}_3$  structure (JCPDS Card No. 01-089-4016). The absence

of K-related peaks is due to the high dispersion of these species on the layered-double hydroxide support (Wang et al., 2001; Boukha et al., 2010).

STEM and EDX mapping were performed to further investigate the effect of the promoter on the nickel location and particle size (Figure 4). The EDX mapping of the three catalysts showed that nickel was distributed uniformly on the MgAl support without a clear distinction of particles. These findings are in line with previous studies, which demonstrated the formation of  $\text{NiAl}_2\text{O}_4$  and  $\text{Mg}_2\text{AlO}_4$  spinels as mentioned in the XRD analysis (Sahli et al., 2006; Touahra et al., 2016; Ranjbar et al., 2019; Warmuz and Madej, 2022). Based on the STEM images, the average Ni particle size in the 10Ni/MgAl catalyst was about 8.6 nm. In comparison, La-promoted catalysts had a smaller nickel particle size of 6.4 nm with a narrow distribution. Similarly, the K-promoted catalyst showed a reduced nickel particle size of 7.3 nm. The average Ni particle size decreased over the La/K- modified Ni catalysts, which is in line with the change in Ni particle size calculated from the XRD analysis. The decrease in nickel particle size is a key factor responsible for the different activities of the K and La-promoted catalysts.

The interaction between the Ni and the MgAl support is an important factor in the catalyst performance. Figure 5 and Supplementary Table S1 showed the  $\text{H}_2$ -TPR profiles of MgAl support and the calcined Ni-M/MgAl catalysts.  $\text{Ni}^{2+}$  species have been shown to be reduced between  $350$  and  $500^\circ\text{C}$  and the reduction temperature generally depends on the Ni dispersion, crystallite size and metal-support interaction (Mikhail et al., 2021). For the 10Ni/MgAl, a broad peak ranging from  $300^\circ\text{C}$ – $900^\circ\text{C}$  was observed, which can be due to the reduction of a small fraction of surface free NiO and  $\text{NiAl}_2\text{O}_4$  spinel. The

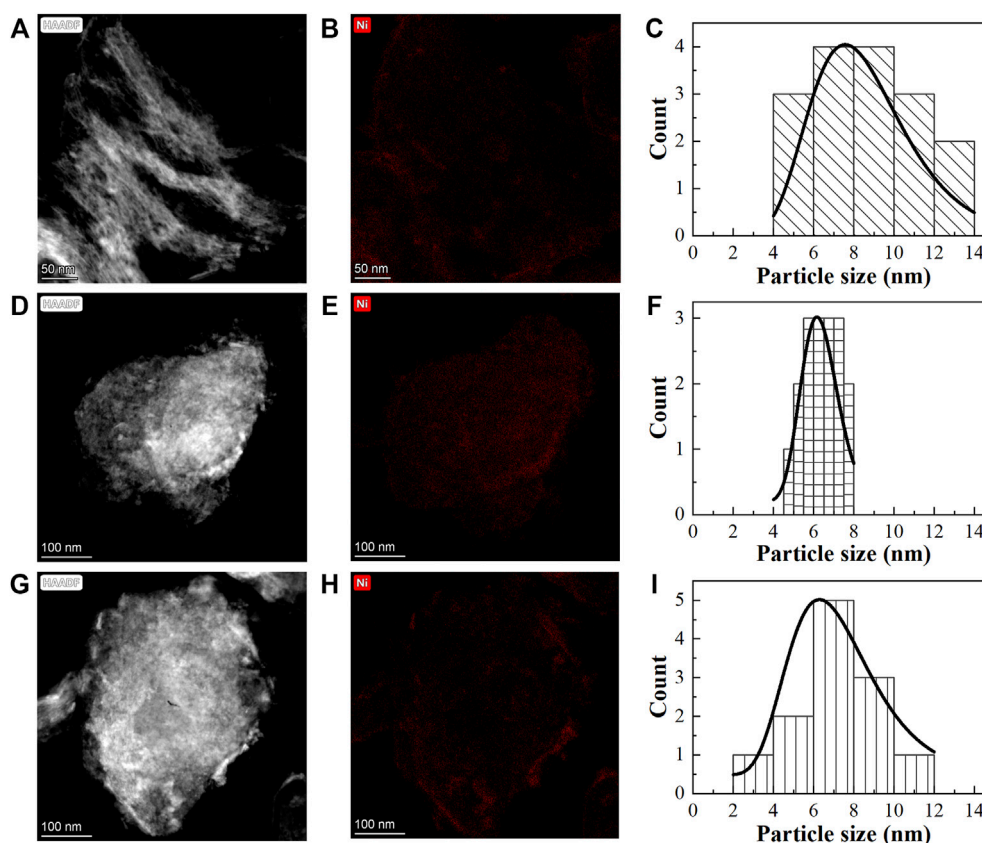


**FIGURE 4**  
STEM images, EDX mapping and the corresponding nickel particle size distribution of (A–C) 10Ni/MgAl, (D–F) 10Ni-5La/MgAl and (G–I) 10Ni-1K/MgAl (Ni particle size was determined by counting >12 particles).

$\text{NiAl}_2\text{O}_4$  phase is formed by  $\text{Ni}^{2+}$  species closely interacting with the MgAl support and hence is reduced at higher temperatures (Rahmani et al., 2014; Morales-Marín et al., 2019). This is in line with the result from EDX mapping in Figure 4. For the La-promoted catalysts (Figure 5A), the reduction peak of  $\text{Ni}^{2+}$  shifted to a lower temperature, indicating that La promoted the reducibility of Ni species (Chen et al., 2019). Specifically, the broad peaks at  $300^\circ\text{C}$ – $500^\circ\text{C}$  and a small asymmetric peak at  $600^\circ\text{C}$  could be related to NiO with small particle size or on the external surface of the MgAl support with weakened Ni-support interaction. Since the lifetime of plasma-activated reactive species is normally short (generally, under atmospheric pressure conditions, the mean free path and time interval between collisions is ca. 100 nm and ca. 1 ns, respectively), easy accessibility of metal active sites on the catalyst surface by plasma-activated reactive species in the gas phase is important in the plasma catalysis (Whitehead, 2019). Thus, such Ni sites on the external surface of the support were beneficial to interact with vibrationally excited  $\text{CO}_2$  species in the gas phase and contributed to the increased  $\text{CO}_2$  conversion. Comparatively, for K-promoted catalysts (Figure 5B), a sharp peak at

$250^\circ\text{C}$ – $500^\circ\text{C}$  can be assigned to the reduction of weakly interacted NiO species or the reduction of  $\text{KNO}_3$  residue on the support (i.e., some  $\text{KNO}_3$  did not decompose during the calcination in the catalyst preparation) (Hleis et al., 2008; Grzybek et al., 2021; Azancot et al., 2022; Greluk et al., 2022). With the K loading increasing from 0.5% to 3%, more NiO can be reduced at low temperatures, indicating that higher K loading increases the Ni reducibility and decreases metal-support interaction. However, K-promoted catalysts showed a decreased  $\text{CO}_2$  conversion in the NTP-catalysis when the K loading increased from 0.5% to 3% (from Figure 2), suggesting that weak interaction of Ni-support is not beneficial for  $\text{CO}_2$  hydrogenation.

XPS analysis was carried out to further investigate the chemical state of Ni species and their interaction with support. Figure 6 shows the Ni 2p and La 3d XP spectra for the reduced 10Ni/MgAl, 10Ni-5La/MgAl and 10Ni-1K/MgAl catalysts. However, the catalysts were partially oxidised due to air exposure before XPS testing. Therefore, the high-resolution XPS spectra of Ni  $2p_{3/2}$  were deconvoluted into two peaks at 855.0 eV (attributed to  $\text{Ni}^{2+}$  in NiO), and at 861.1 eV (associated

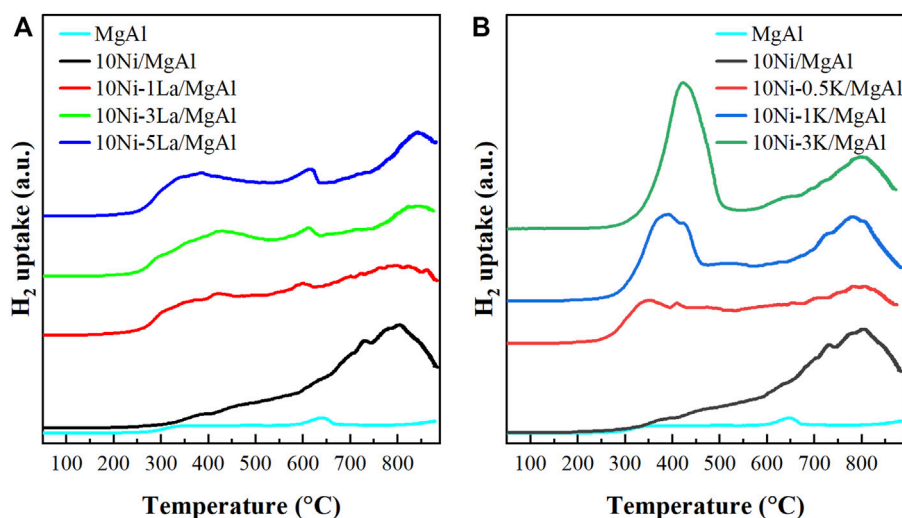


**FIGURE 5**  
H<sub>2</sub>-TPR profiles of the MgAl supporting material, 10Ni/MgAl catalyst, the La-promoted catalysts (A) and the K-modified catalysts (B).

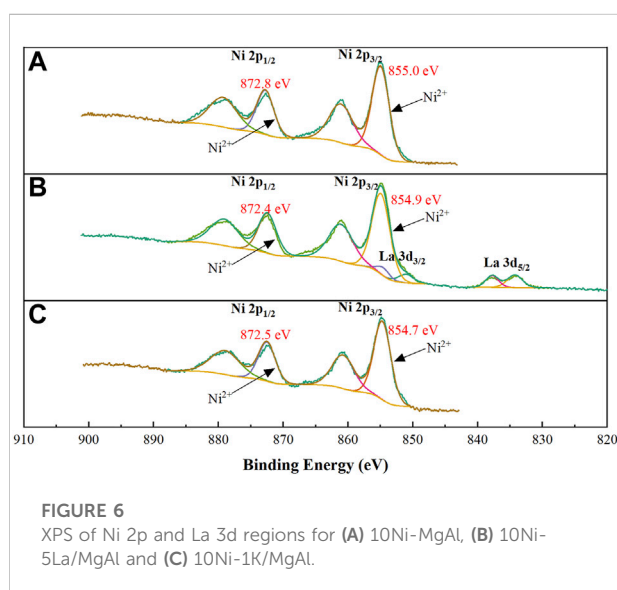


**FIGURE 6**  
XPS of Ni 2p and La 3d regions for (A) 10Ni-MgAl, (B) 10Ni-5La/MgAl and (C) 10Ni-1K/MgAl.

with the satellite peak of Ni<sup>2+</sup>). It was found that the binding energy of Ni 2p is in the following order: 10Ni/MgAl ≈ 10Ni-5La/MgAl > 10Ni-1K/MgAl. This indicated that 10Ni-1K/MgAl catalyst had a relatively weak interaction between Ni NPs and support, which is in line with the H<sub>2</sub>-TPR result (Gao et al., 2019). Additionally, the 10Ni-5La/MgAl catalyst showed La 3d regions, which consisted of a peak at 834.2 eV corresponding to La<sup>3+</sup> species and a satellite peak at 837.7 eV (Chen et al., 2017).

The surface basicity of the Ni-M/MgAl catalysts was evaluated by CO<sub>2</sub>-TPD measurements and shown in Figure 7 and Supplementary Table S2. For all the catalysts, the broad peak

located at 150°C–350°C can be attributed to medium basic sites (Aziz et al., 2020), while another broad peak at 400°C–700°C originated from the complete decomposition of [CO<sub>3</sub>]<sup>2-</sup> species in the internal LDH layer (Xu et al., 2020). After introducing La and K into the Ni catalyst, the CO<sub>2</sub> desorption peak for medium basic sites shifted to a lower temperature, indicating that both promoters weakened the interaction between catalysts and CO<sub>2</sub> molecules. However, the La and K promoters presented different effect on the Ni performance in the plasma catalysis (in Figures 1, 2) and the total amount of CO<sub>2</sub> desorption over all the catalysts are comparable (Supplementary Table S2), indicating that the amount of medium basic sites in each catalyst might not play a key role in the NTP-catalysis.

### 3.3 Mechanistic study of NTP-assisted CO<sub>2</sub> hydrogenation

The reaction mechanism of CO<sub>2</sub> hydrogenation was investigated using *in situ* DRIFTS-MS over the 10Ni/MgAl, 10Ni-5La/MgAl and 10Ni-1K/MgAl catalysts under NTP conditions (Figures 8, Supplementary Figures S6–S10). The 5wt% La and 1wt% K loadings were chosen as they showed main difference in activities compared to the 10Ni/MgAl catalyst in terms of CO<sub>2</sub> conversion and CO/CH<sub>4</sub> selectivity. Three mechanisms have been proposed for CO<sub>2</sub> methanation: (1) CO<sub>2</sub> is transformed into carbonyl (CO) species *via* the reverse water gas shift reaction (RWGS) with the formation of oxygenate species such as the formate (COOH\* or HCOO\*) intermediates (Marwood et al., 1997; Solis-Garcia et al., 2017), (2) surface dissociation of CO<sub>2</sub> to CO\* and atomic oxygen

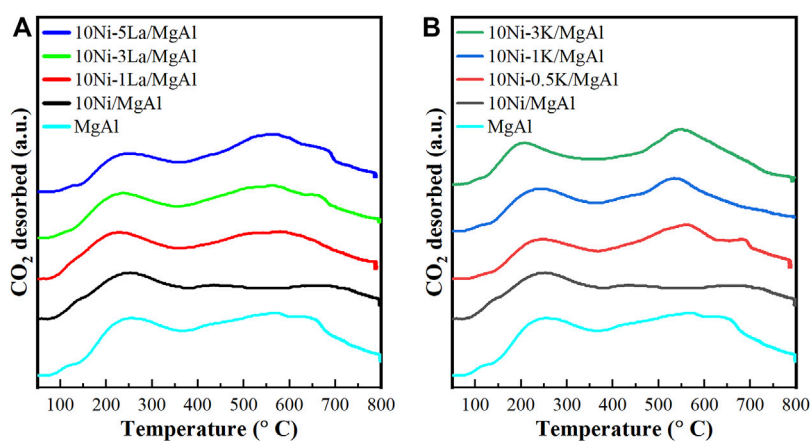


**FIGURE 7**  
CO<sub>2</sub>-TPD profiles of the MgAl supporting material, 10Ni/MgAl catalyst, the La-promoted catalysts (A) and the K-modified catalysts (B).

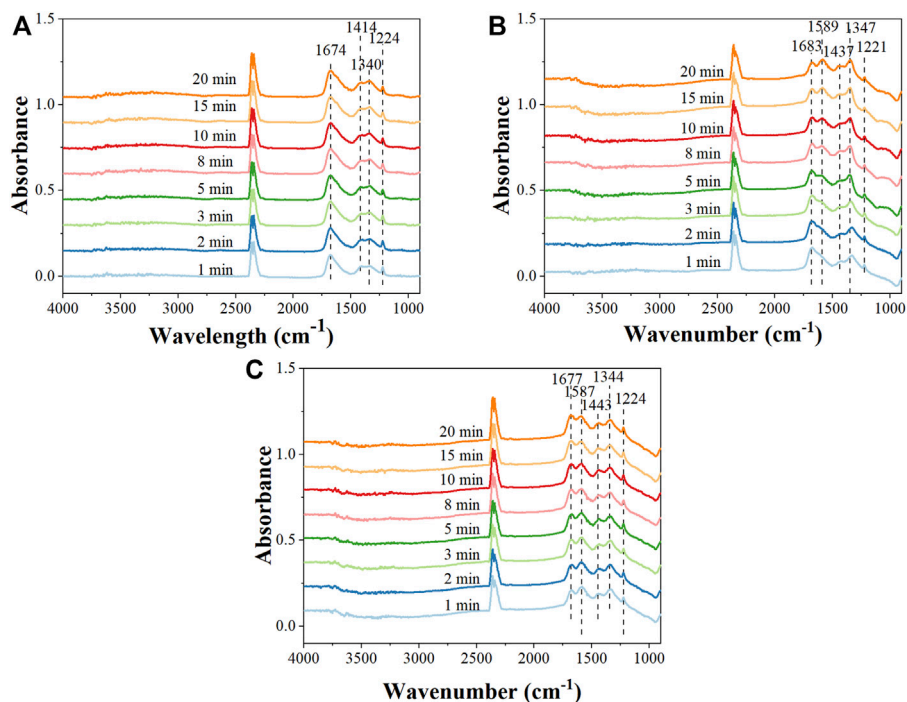


**FIGURE 8**  
*In situ* DRIFTS spectra of surface species on the 10Ni/MgAl catalyst under (A) the gas feed with plasma-off condition, (B) the gas feed and plasma-on condition (5 kV, 27.2 kHz) and (C) the plasma-off condition after the reaction (feed: 2% CO<sub>2</sub> + 8% H<sub>2</sub> + Ar).

followed by hydrogenation of CO\* (Eckle et al., 2011) and (3) dissociation of CO<sub>2</sub>, followed by dissociation of CO\* to C\* and hydrogenation of surface bounded C\* (Ren et al., 2015).

For the 10Ni/MgAl catalyst (Figure 8 and Supplementary Figure S8), with the plasma-off condition, the catalyst was not

active and no CO and CH<sub>4</sub> products were detected. In this condition, IR bands at 1,674 cm<sup>-1</sup> [ $\nu_{as}$ (CO<sub>3</sub>)], 1,414 cm<sup>-1</sup> [ $\nu_s$ (CO<sub>3</sub>)], 1,340 cm<sup>-1</sup> [ $\nu_s$ (CO<sub>3</sub>)], and 1,224 cm<sup>-1</sup> [ $\delta$ (COH)] were observed which correspond to bicarbonate and bidentate carbonate adsorbed on the catalyst surface (Schreiter et al.,

TABLE 1 The ratio of peak area between formate species and bicarbonate species in the steady state recorded from the *in-situ* DRIFTS.

Catalysts	Formate/bicarbonate
10Ni/MgAl	1.5
10Ni-5La/MgAl	1.8
10Ni-1K/MgAl	1.4

2020; Park et al., 2022), which originated from the interaction of CO<sub>2</sub> molecules with oxygen/hydroxyl group (Korhonen et al., 2008). Upon the ignition of plasma, the instantaneous appearance of CH<sub>4</sub> ( $m/z = 15$ ) and CO signal ( $m/z = 28$ ) associated with a decrease of CO<sub>2</sub> signal ( $m/z = 44$ ) in MS profiles (Supplementary Figure S8) confirmed the activity of the NTP-catalysis system. From *in situ* DRIFTS, the IR intensity of bicarbonate species at 1,683 cm<sup>-1</sup> [ $\nu_{as}(\text{CO}_3)$ ] was found to decrease gradually, while another three bands located at 1,589 cm<sup>-1</sup> [ $\nu_{as}(\text{HCOO})$ ], 1,437 cm<sup>-1</sup> (CH bending) and 1,347 cm<sup>-1</sup> [ $\nu_s(\text{HCOO})$ ], corresponding to formate species adsorbed on the surface of the catalyst (Pan et al., 2014), appeared and their intensity continuously increased with time. This confirmed that the carbonate species were transformed to formate under plasma and CO<sub>2</sub> hydrogenation over 10 Ni/MgAl catalyst was via the formate pathway (Aldana et al., 2013). When the plasma was extinguished again, the MS profile showed that the system was not active (Supplementary Figure S8). However, the adsorbed formate species remained on the Ni surface due to the strong adsorption.

For 10Ni-5La/MgAl and 10Ni-1K/MgAl catalysts, the MS profiles (Supplementary Figures S9, S10) demonstrated a similar synergetic effect of the plasma-catalyst system. Interestingly, on comparing the DRIFTS spectra for the 10Ni/MgAl catalysts, the La and K promoters were shown to affect the binding of formate on the Ni surface. This is evidenced by the band shift from 1,683, 1,437 and 1,347 cm<sup>-1</sup> to 1,665, 1,408 and 1,318 cm<sup>-1</sup>, suggesting a stronger interaction between the formate species and Ni surface over the 10Ni-5La/MgAl and 10Ni-1K/MgAl catalysts. Additionally, 10Ni-5La/MgAl catalyst showed a high formate/bicarbonate ratio of 1.8 in the steady state compared with the 10Ni/MgAl and 10Ni-1K/MgAl catalysts of 1.4–1.5 (Table 1), which indicated that La could facilitate the formation of formate and K showed no effect on this process. This is consistent with their performance regarding CO<sub>2</sub> conversion in NTP-activated CO<sub>2</sub> hydrogenation. It is, therefore, proposed that the NTP-promoted CO<sub>2</sub> hydrogenation occurs *via* the formate pathway over all the catalysts; however, the La and K promoters affect the interaction and amount of formate intermediate, thus affecting the activity of Ni/MgAl catalysts.

## 4 Conclusion

A range of Ni catalysts supported on layered-double hydroxides modified with La and K were prepared and tested for CO<sub>2</sub> hydrogenation under NTP conditions, where CO<sub>2</sub> conversion and product selectivity can be successfully tuned over promoted Ni catalysts. Compared with the unpromoted Ni catalyst, the introduction of La as the promoter resulted in a significant increase in the CO<sub>2</sub> conversion and CH<sub>4</sub> selectivity at low applied voltages, while the use of K as the promoter did not affect the CO<sub>2</sub> conversion but significantly increased CO selectivity. Comparing the structural characteristics of the catalysts showed that the nickel particle size and the interaction between metal and support are affected by the promoter and this affects the activity. The promoters used (La and K) contributed to 1) a decreased Ni particle size and higher Ni dispersion on the layered-double hydroxide support 2) a reduced Ni-supported interaction and 3) an enhanced formation of formate intermediate for CO/CH<sub>4</sub> production. This work demonstrated the effect of the promoter on the catalyst design for the NTP-assisted CO<sub>2</sub> hydrogenation and exemplified that further work is required to understand the activity of complex catalyst systems.

## Data availability statement

The original contributions presented in the study are included in the article/Supplementary Material, further inquiries can be directed to the corresponding authors. Open access data can be found via the University of Manchester research portal.

## Author contributions

CC carried out all experimental work and data interpretation under the supervision of AG, CH, JG, and SX. SX contributed to the *in situ* DRIFTS-MS characterisation and data interpretation under the supervision of AG and CH. SD and AL contributed to the TEM characterisation under the supervision of CP. SC contributed to the XPS characterisation under the supervision of CH. EA contributed to the TGA characterisation under the supervision of AG.

## Funding

The University of Manchester are thanked for the funding of CC's PhD studentship. UK Catalysis Hub is kindly thanked for resources and support provided *via* our membership of the UK Catalysis Hub Consortium and funded by EPSRC Grants: EP/R026939/1, EP/R026815/1, EP/R026645/1, and EP/R027129/1.

## Conflict of interest

The authors declare that the research was conducted in the absence of any commercial or financial relationships that could be construed as a potential conflict of interest.

## Publisher's note

All claims expressed in this article are solely those of the authors and do not necessarily represent those of their affiliated

organizations, or those of the publisher, the editors and the reviewers. Any product that may be evaluated in this article, or claim that may be made by its manufacturer, is not guaranteed or endorsed by the publisher.

## Supplementary material

The Supplementary Material for this article can be found online at: <https://www.frontiersin.org/articles/10.3389/fceng.2022.1027167/full#supplementary-material>

## References

- Aldana, P. A. U., Ocampo, F., Kobl, K., Louis, B., Thibault-Starzyk, F., Daturi, M., Bazin, P., Thomas, S., and Roger, A. C. (2013). Catalytic CO<sub>2</sub> valorization into CH<sub>4</sub> on Ni-based ceria-zirconia. Reaction mechanism by operando IR spectroscopy. *Catal. Today* 215, 201–207. doi:10.1016/j.cattod.2013.02.019
- Azancot, L., Blay, V., Blay-Roger, R., Bobadilla, L. F., Penkova, A., Centeno, M. A., et al. (2022). Evidence of new Ni-O-K catalytic sites with superior stability for methane dry reforming. *Appl. Catal. B: Environ.* 307, 121148. doi:10.1016/j.apcatb.2022.121148
- Aziz, M. A. A., Jalil, A. A., Wongsakulphasatch, S., and Vo, D.-V. N. (2020). Understanding the role of surface basic sites of catalysts in CO<sub>2</sub> activation in dry reforming of methane: A short review. *Catal. Sci. Technol.* 10 (1), 35–45. doi:10.1039/C9CY01519A
- Benrababah, R., Cavaniol, C., Liu, H., Ognier, S., Cavadias, S., Gálvez, M. E., and Da Costa, P. (2017). Plasma DBD activated ceria-zirconia-promoted Ni-catalysts for plasma catalytic CO<sub>2</sub> hydrogenation at low temperature. *Catal. Commun.* 89, 73–76. doi:10.1016/j.catcom.2016.10.028
- Bogaerts, A., and Centi, G. (2020). Plasma technology for CO<sub>2</sub> conversion: A personal perspective on prospects and gaps. *Front. Energy Res.* 8. doi:10.3389/fenrg.2020.00111
- Boukha, Z., Fitian, L., López-Haro, M., Mora, M., Ruiz, J. R., Jiménez-Sanchidrián, C., Blanco, G., Calvino, J.J., Cifredo, G.A., Trasobares, S., and Bernal, S. (2010). Influence of the calcination temperature on the nanostructural properties, surface basicity, and catalytic behavior of alumina-supported lanthana samples. *J. Catal.* 272 (1), 121–130. doi:10.1016/j.jcat.2010.03.005
- Chen, G., Snyders, R., and Britun, N. (2021). CO<sub>2</sub> conversion using catalyst-free and catalyst-assisted plasma-processes: Recent progress and understanding. *J. CO<sub>2</sub> Util.* 49, 101557. doi:10.1016/j.jcou.2021.101557
- Chen, H., Mu, Y., Shao, Y., Chansai, S., Xu, S., Stere, C. E., Xiang, H., Zhang, R., Jiao, Y., Hardacre, C., and Fan, X. (2019). Coupling non-thermal plasma with Ni catalysts supported on BETA zeolite for catalytic CO<sub>2</sub> methanation. *Catal. Sci. Technol.* 9 (15), 4135–4145. doi:10.1039/c9cy00590k
- Chen, H., Mu, Y., Xu, S., Xu, S., Hardacre, C., and Fan, X. (2020). Recent advances in non-thermal plasma (NTP) catalysis towards C1 chemistry. *Chin. J. Chem. Eng.* 28 (8), 2010–2021. doi:10.1016/j.cjche.2020.05.027
- Chen, S., Pan, B., Zeng, L., Luo, S., Wang, X., and Su, W. (2017). La<sub>2</sub>Sn<sub>2</sub>O<sub>7</sub> enhanced photocatalytic CO<sub>2</sub> reduction with H<sub>2</sub>O by deposition of Au co-catalyst. *RSC Adv.* 7 (23), 14186–14191. doi:10.1039/C7RA00765E
- Choi, P. H., Jun, K. W., Lee, S. J., Choi, M. J., and Lee, K. W. (1996). Hydrogenation of carbon dioxide over alumina supported Fe-K catalysts. *Catal. Lett.* 40 (1), 115–118. doi:10.1007/BF00807467
- Cimino, S., Boccia, F., and Lisi, L. (2020). Effect of alkali promoters (Li, Na, K) on the performance of Ru/Al<sub>2</sub>O<sub>3</sub> catalysts for CO<sub>2</sub> capture and hydrogenation to methane. *J. CO<sub>2</sub> Util.* 37, 195–203. doi:10.1016/j.jcou.2019.12.010
- Da Costa, P., Hasrack, G., Bonnetty, J., and Henriques, C. (2021). Ni-based catalysts for plasma-assisted CO<sub>2</sub> methanation. *Curr. Opin. Green Sustain. Chem.* 32, 100540. doi:10.1016/j.cogsc.2021.100540
- Du, C., Wang, X., Chen, W., Feng, S., Wen, J., and Wu, Y. A. (2020). CO<sub>2</sub> transformation to multicarbon products by photocatalysis and electrocatalysis. *Mater. Today Adv.* 6, 100071. doi:10.1016/j.mtadv.2020.100071
- Eckle, S., Anfang, H.-G., and Behm, R. J. (2011). Reaction intermediates and side products in the methanation of CO and CO<sub>2</sub> over supported Ru catalysts in H<sub>2</sub>-rich reformat gases. *J. Phys. Chem. C* 115 (4), 1361–1367. doi:10.1021/jp108106t
- Gao, R., Pan, L., Wang, H., Yao, Y., Zhang, X., Wang, L., et al. (2019). Breaking trade-off between selectivity and activity of nickel-based hydrogenation catalysts by tuning both steric effect and d-band center. *Adv. Sci. (Weinh.)* 6 (10), 1900054. doi:10.1002/advs.201900054
- George, A., Shen, B., Craven, M., Wang, Y., Kang, D., Wu, C., et al. (2021). A review of non-thermal plasma technology: A novel solution for CO<sub>2</sub> conversion and utilization. *Renew. Sustain. Energy Rev.* 135, 109702. doi:10.1016/j.rser.2020.109702
- Greluk, M., Rotko, M., Słowik, G., Turczyniak-Surdacka, S., Grzybek, G., Góra-Marek, K., et al. (2022). Effect of Potassium Promoter on the Performance of Nickel-Based Catalysts Supported on MnO<sub>x</sub> in Steam Reforming of Ethanol. *Catalysts* 12 (6). doi:10.3390/catal12060600
- Grzybek, G., Góra-Marek, K., Patulski, P., Greluk, M., Rotko, M., Słowik, G., et al. (2021). Optimization of the potassium promotion of the Co/α-Al<sub>2</sub>O<sub>3</sub> catalyst for the effective hydrogen production via ethanol steam reforming. *Appl. Catal. A: General* 614, 118051. doi:10.1016/j.apcata.2021.118051
- He, S., An, Z., Wei, M., Evans, D. G., and Duan, X. (2013). Layered double hydroxide-based catalysts: Nanostructure design and catalytic performance. *Chem. Commun.* 49 (53), 5912–5920. doi:10.1039/c3cc42137f
- Hleis, D., Labaki, M., Laversin, H., Courcot, D., and Aboukais, A. (2008). Comparison of alkali-promoted ZrO<sub>2</sub> catalysts towards carbon black oxidation. *Colloids Surf. A Physicochem. Eng. Aspects* 330 (3), 193–200. doi:10.1016/j.colsurfa.2008.07.052
- Korhonen, S. T., Calatayud, M., and Krause, A. O. I. (2008). Structure and stability of formates and carbonates on monoclinic zirconia: A combined study by density functional theory and infrared spectroscopy. *J. Phys. Chem. C* 112 (41), 16096–16102. doi:10.1021/jp803353v
- Kumar, K. D. P. L., Naidu, B. N., Sarkar, B., Mondal, P., Ghosh, K., and Prasad, V. V. D. N. (2021). Enhanced CO<sub>2</sub> utilization via methane tri-reforming over Ru incorporated Co/MgO-Al<sub>2</sub>O<sub>3</sub> catalyst: Influence of La and Ce promoters. *J. Environ. Chem. Eng.* 9 (5), 105949. doi:10.1016/j.jece.2021.105949
- Li, W., Wang, H., Jiang, X., Zhu, J., Liu, Z., Guo, X., et al. (2018). A short review of recent advances in CO<sub>2</sub> hydrogenation to hydrocarbons over heterogeneous catalysts. *RSC Adv.* 8 (14), 7651–7669. doi:10.1039/c7ra13546g
- Marwood, M., Doepper, R., and Renken, A. (1997). *In-situ* surface and gas phase analysis for kinetic studies under transient conditions the catalytic hydrogenation of CO<sub>2</sub>. *Appl. Catal. A General* 151 (1), 223–246. doi:10.1016/S0926-860X(96)00267-0
- Mikhail, M., Costa, P. D., Amouroux, J., Cavadias, S., Tatoulian, M., Ognier, S., et al. (2021). Effect of Na and K impurities on the performance of Ni/CeZrO<sub>x</sub> catalysts in DBD plasma-catalytic CO<sub>2</sub> methanation. *Fuel* 306, 121639. doi:10.1016/j.fuel.2021.121639
- Morales-Marín, A., Ayastuy, J. L., Iriarte-Velasco, U., and Gutiérrez-Ortiz, M. A. (2019). Nickel aluminate spinel-derived catalysts for the aqueous phase reforming of glycerol: Effect of reduction temperature. *Appl. Catal. B Environ.* 244, 931–945. doi:10.1016/j.apcatb.2018.12.020
- Pan, Q., Peng, J., Sun, T., Wang, S., and Wang, S. (2014). Insight into the reaction route of CO<sub>2</sub> methanation: Promotion effect of medium basic sites. *Catal. Commun.* 45, 74–78. doi:10.1016/j.catcom.2013.10.034

- Park, S. J., Wang, X., Ball, M. R., Proano, L., Wu, Z., and Jones, C. W. (2022). CO<sub>2</sub> methanation reaction pathways over unpromoted and NaNO<sub>3</sub>-promoted Ru/Al<sub>2</sub>O<sub>3</sub> catalysts. *Catal. Sci. Technol.* 12 (14), 4637–4652. doi:10.1039/D2CY00515H
- Petersen, E. M. (2019). *Fueling the mission to mars and earth's transition to renewable energy. increasing catal. perform. carbon dioxide methanation*. Doctoral dissertation, Iowa State University, Ames, IA, USA
- Rahmani, S., Rezaei, M., and Meshkani, F. (2014). Preparation of highly active nickel catalysts supported on mesoporous nanocrystalline  $\gamma$ -Al<sub>2</sub>O<sub>3</sub> for CO<sub>2</sub> methanation. *J. Industrial Eng. Chem.* 20 (4), 1346–1352. doi:10.1016/j.jiec.2013.07.017
- Ranjbar, A., Irankhah, A., and Aghamiri, S. F. (2019). Catalytic activity of rare Earth and alkali metal promoted (Ce, La, Mg, K) Ni/Al<sub>2</sub>O<sub>3</sub> nanocatalysts in reverse water gas shift reaction. *Res. Chem. Intermed.* 45 (10), 5125–5141. doi:10.1007/s11164-019-03905-1
- Ren, J., Guo, H., Yang, J., Qin, Z., Lin, J., and Li, Z. (2015). Insights into the mechanisms of CO<sub>2</sub> methanation on Ni(111) surfaces by density functional theory. *Appl. Surf. Sci.* 351, 504–516. doi:10.1016/j.apsusc.2015.05.173
- Rosset, M., F  ris, L. A., and Perez-Lopez, O. W. (2021). Biogas dry reforming over Ni-M-Al (M = K, Na and Li) layered double hydroxide-derived catalysts. *Catal. Today* 381, 96–107. doi:10.1016/j.cattod.2020.08.018
- Sahli, N., Petit, C., Roger, A. C., Kiennemann, A., Libs, S., and Bettahar, M. M. (2006). Ni catalysts from NiAl<sub>2</sub>O<sub>4</sub> spinel for CO<sub>2</sub> reforming of methane. *Catal. Today* 113 (3–4), 187–193. doi:10.1016/j.cattod.2005.11.065
- Samplatsky, D., Grohs, K., Edeen, M., Crusan, J., and Burkey, R. (2011). Development and integration of the flight sabatier assembly on the ISS. *41st Int. Conf. Environ. Syst.* doi:10.2514/6.2011-5151
- Schreiter, N., Kirchner, J., and Kureti, S. (2020). A DRIFTS and TPD study on the methanation of CO<sub>2</sub> on Ni/Al<sub>2</sub>O<sub>3</sub> catalyst. *Catal. Commun.* 140, 105988. doi:10.1016/j.catcom.2020.105988
- Solis-Garcia, A., Louvier-Hernandez, J. F., Almendarez-Camarillo, A., and Fierro-Gonzalez, J. C. (2017). Participation of surface bicarbonate, formate and methoxy species in the carbon dioxide methanation catalyzed by ZrO<sub>2</sub>-supported Ni. *Appl. Catal. B Environ.* 218, 611–620. doi:10.1016/j.apcatb.2017.06.063
- Stere, C., Chansai, S., Gholami, R., Wangkawong, K., Singhanian, A., Goguet, A., et al. (2020). A design of a fixed bed plasma DRIFTS cell for studying the NTP-assisted heterogeneously catalysed reactions. *Catal. Sci. Technol.* 10 (5), 1458–1466. doi:10.1039/D0CY00036A
- Touahra, F., Sehalia, M., Ketir, W., Bachari, K., Chebout, R., Trari, M., et al. (2016). Effect of the Ni/Al ratio of hydrotalcite-type catalysts on their performance in the methane dry reforming process. *Appl. Petrochem. Res.* 6 (1), 1–13. doi:10.1007/s13203-015-0109-y
- Tu, W., Zhou, Y., and Zou, Z. (2014). Photocatalytic conversion of CO<sub>2</sub> into renewable hydrocarbon fuels: State-of-the-Art accomplishment, challenges, and prospects. *Adv. Mat.* 26 (27), 4607–4626. doi:10.1002/adma.201400087
- Vogt, C., Monai, M., Kramer, G. J., and Weckhuysen, B. M. (2019). The renaissance of the Sabatier reaction and its applications on Earth and in space. *Nat. Catal.* 2 (3), 188–197. doi:10.1038/s41929-019-0244-4
- Wang, Y., Huang, W. Y., Chun, Y., Xia, J. R., and Zhu, J. H. (2001). Dispersion of potassium nitrate and the resulting strong basicity on zirconia. *Chem. Mat.* 13 (2), 670–677. doi:10.1021/cm000213n
- Warmuz, K., and Madej, D. (2022). Synthesis and evaluation of Mg-Al hydrotalcite formation and its influence on the microstructural evolution of spinel-forming refractory castables under intermediate temperatures. *J. Eur. Ceram. Soc.* 42 (5), 2545–2555. doi:10.1016/j.jeurceramsoc.2022.01.009
- Wei, Z., Qiao, H., Yang, H., Zhang, C., and Yan, X. (2009). Characterization of NiO nanoparticles by anodic arc plasma method. *J. Alloys Compd.* 479 (1–2), 855–858. doi:10.1016/j.jallcom.2009.01.064
- Whitehead, J. C. (2019). Plasma-catalysis: Is it just a question of scale? *Front. Chem. Sci. Eng.* 13 (2), 264–273. doi:10.1007/s11705-019-1794-3
- Whitehead, J. C. (2016). Plasma-catalysis: The known knowns, the known unknowns and the unknown unknowns. *J. Phys. D: Appl. Phys.* 49 (24), 243001. doi:10.1088/0022-3727/49/24/243001
- Xu, S., Chansai, S., Shao, Y., Xu, S., Wang, Y.-c., Haigh, S., et al. (2020). Mechanistic study of non-thermal plasma assisted CO<sub>2</sub> hydrogenation over Ru supported on MgAl layered double hydroxide. *Appl. Catal. B Environ.* 268, 118752. doi:10.1016/j.apcatb.2020.118752
- Xu, S., Chen, H., Hardacre, C., and Fan, X. (2021). Non-thermal plasma catalysis for CO<sub>2</sub> conversion and catalyst design for the process. *J. Phys. D: Appl. Phys.* 54 (23), 233001. doi:10.1088/1361-6463/abe9e1
- Zeng, Y. X., Wang, L., Wu, C. F., Wang, J. Q., Shen, B. X., and Tu, X. (2018). Low temperature reforming of biogas over K-Mg- and Ce-promoted Ni/Al<sub>2</sub>O<sub>3</sub> catalysts for the production of hydrogen rich syngas: Understanding the plasma-catalytic synergy. *Appl. Catal. B Environ.* 224, 469–478. doi:10.1016/j.apcatb.2017.10.017